Inorganic Chemistry

Article

pubs.acs.org/IC

Illustrating the Processability of Magnetic Layered Double Hydroxides: Layer-by-Layer Assembly of Magnetic Ultrathin Films

E. Coronado,[†] C. Martí-Gastaldo,*[,†,‡] E. Navarro-Moratalla,[†] A. Ribera,*[,†] and S. Tatay[†,§]

[†]Instituto de Ciencia Molecular (ICMol), Universidad de Valencia, Catedrático José Beltrán 2, 46890 Paterna, Spain

[‡]Department of Chemistry, University of Liverpool, Crown Street, L697ZD Liverpool, United Kingdom

[§]Unité Mixte de Physique CNRS/Thales (UMR137), Associée à l'Université Paris-Sud 11, Augustin Fresnel, 1, 91767 Palaiseau cedex, France

Supporting Information

ABSTRACT: We report the preparation of single-layer layered double hydroxide (LDH) two-dimensional (2D) nanosheets by exfoliation of highly crystalline NiAl-NO_3 LDH. Next, these unilamellar moieties have been incorporated layer-by-layer (LbL) into a poly(sodium 4-styrenesulfonate)/LDH nanosheet multilayer ultrathin film (UTF). Fourier transform infrared spectroscopy (FT-IR), ultraviolet−visible light (UV−vis), and X-ray diffraction (XRD) profiles have been used to follow the uniform growth of the UTF. The use of a magnetic LDH as the cationic component of the multilayered architecture enables study of the resulting magnetic properties of the UTFs. Our magnetic data show the appearance of spontaneous magnetization at ∼5 K, thus confirming the effective transfer of the magnetic properties of the bulk LDH to the self-assembled film that displays glassy-like ferromagnetic behavior. The high number of bilayers accessible—more than 80—opens the door for the preparation of more-complex hybrid multifunctional materials that combine magnetism with the physical properties provided by other exfoliable layered inorganic hosts.

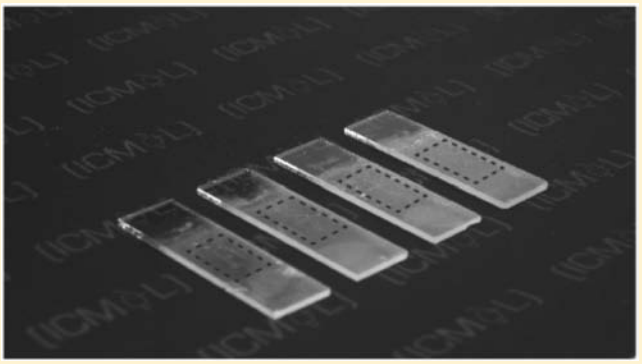

INTRODUCTION

Alongside the design of novel magnetic systems, one of the current goals of molecular magnetism is to gain control of the organization of discrete and extended magnetic nanoobjects onto surfaces or hierarchically incorporated into three-dimensional (3D) superstructures. To date, the development of novel processing techniques has enabled the production of two-dimensional (2D) nanostructures via the patterning of single molecule magnets (SMMs) or magnetic nanoparticles onto solid substrates.[1−5] Even more, we recently demonstrated how room-temperature magnetic oxides could be nanostructured via the lithographically controlled wetting (LCW) of soluble molecular magnets onto SiO_2.[6] As for the fabrication of 3D multilayered films, the Langmuir−Blodgett (LB) technique has been the most widely used route, because it favors the processing of molecules into magnetic or conducting thin films while controlling their 2D structure at the molecular level.[7−9] Still, most of these examples rely on the use of zero-dimensional (0D) molecular components, although the processing of 2D magnetic single layers offers a geometrical advantage that favors their processability over their lower dimensional 0D and one-dimensional (1D) counterparts.

Layered double hydroxides (LDHs), commonly known as hydrotalcite-like compounds or anionic clays, are a group of minerals described by the formula $[M^{II}_{1-x}M^{III}_{x}(OH)_2](A^{n-})_{x/n}\cdot mH_2O$, where M^{II} and M^{III} correspond to divalent and trivalent metal ions ($0.20 \le x \le 0.33$), A^{n-} is an interlayer anion and m corresponds to the number of water molecules.[10] From a structural point of view, these materials are equivalent to the mineral brucite, $Mg(OH)_2$, except for the partial substitution of M^{II} with M^{III} ions, which results in the introduction of an excess of net positive charge across the hydroxide layers, which must be balanced by exchangeable interlayer anions for electroneutrality.[11] The structure is additionally stabilized by electronic interactions between the positively charged brucite-like layers and the anions, together with a network of hydrogen bonding interactions comprising hydroxyl slabs, interlayer water molecules, and anions.[12] The exfoliation of LDH materials yields well-defined, micrometric, positively charged nanosheets that retain the physical and chemical properties intrinsic to the layered host.[13] In a next step, these discrete 2D single layers can be used as macromolecular building blocks[14] to synthesize a wide diversity of multifunctional inorganic−organic hybrid nanocomposites, inorganic−inorganic heterogeneous nanomaterials, or novel nanostructures.[15−18] In this context it is worth outlining our recent success in combining two physical properties tradition-

Received: March 25, 2013
Published: April 26, 2013

   dx.doi.org/10.1021/ic400734t | Inorg. Chem. 2013, 52, 6214−6222

ally considered inimical to each other, such as superconductivity and magnetism, in $[Ni_{0.66}Al_{0.33}(OH)_2][TaS_2]$ by chemical design.[15] This multilayered assembly is built-up from the stacking of cationic ferromagnetic (NiAl-LDH) and anionic superconducting (reduced tantalum calchogenide) 2D nanosheets with opposite charge, and it is prepared via direct flocculation of the exfoliated components in organic solvents. Its versatility notwithstanding, this approach suffers from the intrinsic restrictions to rapid precipitation and control on the morphology and crystallinity of the resulting solids is rather limited. Among the potential alternatives that permit directing the controlled assembly of these exfoliated LDH layers into multilayered architectures, "layer-by-layer" (LbL) is arguably the most successful technique. Hence, LbL is ideally suited to construct multilayered films by sequential deposition of positively and negatively charged particles onto solid substrates. This adds processability to the resulting materials, which is of utmost importance for their integration in the forthcoming technological applications.

Since the beginning of the 1990s, when Decher et al.[19] rediscovered the seminal work of Iler,[20] the scientific community has demonstrated an incipient interest for this technique as a versatile tool for the preparation of a wide range of multilayered materials.[21−24] However, among all the examples published, the work of Sasaki et al.[25] reporting the design of hybrid multilayered films of TiO_2 and other transition-metal oxides via LbL has been probably the responsible of giving true relevance to this technique. Concerning LDHs, after well-defined exfoliation methodology was set, an important number of inorganic−organic hybrid nanocomposites, exploiting the advantages offered by the LbL technique, have been described.[26−29] In this context, the work of Duan et al., in which these hybrid materials were endowed with luminescent properties through the incorporation of transition-metal-based photoactive complexes between the LDH-nanosheets,[30] as well as the more recent works appeared about the LbL, providing new applications to these materials,[31−35] are particularly relevant.

Here, we report the controlled LbL assembly of magnetic poly(sodium 4-styrenesulfonate)/LDH multilayered ultrathin films (UTFs) via the introduction of magnetic NiAl-LDH anionic 2D nanosheets. After confirming the success of the LbL deposition process and identifying the structural and morphological features of the $(PSS/NiAl)_n$ architecture, we will focus on its magnetic properties. We will compare the magnetism of the bulk LDH host and the UTF to confirm that both exhibit analogous magnetic behavior, thus illustrating the ability of LDH nanosheets to retain the physical properties intrinsic to the pristine macroscopic solid and act as suitable vehicles to transfer these to more-complex architectures.

EXPERIMENTAL SECTION

1. Synthesis and Exfoliation of LDHs. All chemicals and solvents were from commercial suppliers and were used as received, without further purification. NiAl-LDH was synthesized according to a homogeneous precipitation method,[13d] using hexamethylenetetramine (HMT) as an ammonium-releasing reagent, in order to increase the pH and reach the optimum value for the precipitation of the NiAl double hydroxide.

Synthesis of NiAl-CO_3 LDH (1). The chloride salts of the metals were dissolved in Milli-Q water, with the total metal cation concentration in the final solution being 0.15 M and the ratio between Ni and Al concentration being 2. Next, an aqueous solution of HMT with a concentration three times higher than $[Al^{3+}]$ was added over the metal solution. The resulting green mixture was introduced in a Teflon inner vessel within a stainless steel outer autoclave. It was placed in a preheated oven at 140 °C, and the mixture was allowed to react under airtight conditions. After 72 h, the autoclave was removed from the oven and cooled on a bench to room temperature. The resulting green solid was filtrated, washed thoroughly with distilled water, and dried under vacuum. Infrared (IR) analysis (KBr pellet), ν/cm^{-1}: 3411 (br, st), 1612 (m), 1375 (sh, m), 673 (st), 426 (sh, m). Energy-dispersive X-ray analsis (EDAX) (calculated for $Ni_{0.66}Al_{0.33}$): Found: Ni = 62.2% (66.6%); Al = 37.8% (33.3%). Water content (via thermogravimetry, TG): 5.66%. $[Ni_{0.62}Al_{0.38}(OH)_2](CO_3)_{0.190}\cdot 0.3H_2O$ (formula weight, F_w = 97.63).

Preparation of NiAl-NO_3 (2). The carbonate anions occupying the interlayer space of these LDH precursors were exchanged with nitrate, according to the salt-acid method.[36] In a typical preparation, 0.5 g of the LDH precursor were immersed in a round-bottom flask containing 0.5 L of an aqueous solution of $NaNO_3$ (1.5 M) and HNO_3 (5 mM). The mixture was mechanically stirred under inert atmosphere during 48 h. Finally, the exchanged LDHs were filtered, washed thoroughly with distilled water, and dried under vacuum. IR (KBr pellet), ν/cm^{-1}: 3405 (br, st), 1591 (m), 1342 (sh, m), 779 (st), 403 (sh, m). EDAX (calculated for $Ni_{0.66}Al_{0.33}$): Found Ni = 62.8% (66.6%); Al = 37.2% (33.3%). Water content (TG): 6.82%. $[Ni_{0.63}Al_{0.37}(OH)_2](NO_3)_{0.370}\cdot 0.4H_2O$ (F_w = 111.47).

Exfoliation of NiAl-NO_3. The exchanged nitrate LDH was finely ground and dispersed under an argon atmosphere in degassed formamide at a concentration of 1 g L^{-1}. The mixture then was vigorously stirred for 20 min and sonicated (Branson 5510 ultrasonic water bath, 180 W, 40 kHz) three times in successive intervals of 5 min. Following this treatment, the solution was mechanically stirred under an argon atmosphere for 72 h. Finally, the resulting translucent colloidal suspension was centrifuged at 2000 rpm for 10 min, to ensure that nonexfoliated particles were eliminated.

2. Restacking of LDHs. Reconstitution of the NiAl-LDH systems with poly(sodium 4-styrenesulfonate) (PSS) intercalated in the interlayer space (**3**) was carried out by following a flocculation method. First, freshly prepared colloidal suspensions of delaminated LDH in formamide (1 g L^{-1}) and PSS aqueous solution (prepared by diluting 6 g L^{-1} of a 30 wt % water solution in Milli-Q water) were purged in an argon atmosphere. This procedure avoids the presence of carbonate anions, which could act as reconstructive anion for the cationic nanosheets of LDH in suspension. Next, 200 mL of the delaminated LDH was added onto 200 mL of the solution containing the anionic PSS polymer. Rapid formation of a green precipitate was observed. After finishing the addition process, the stirring was kept for 15 min and the mixture was left to stand at room temperature overnight. The products were isolated by filtration, thoroughly washed with water, and dried at room temperature under vacuum. IR (KBr pellet), ν/cm^{-1}: 3406 (br, st); 2917 (m), 1390 (st), 1176 (m), 1126 (m), 1040 (m), 1008 (m), 771 (m), 673 (m), 642 (m), 402 (st). EDAX (calculated for $Ni_{0.66}Al_{0.33}$): Found Ni = 64.8% (66.66%); Al = 35.2% (33.33%). Water content (TG): 8.89%. $[Ni_{0.65}Al_{0.35}(OH)_2](PSS)_{0.350}\cdot 0.8H_2O$ (F_w = 159.94).

3. LbL Deposition Process. First, quartz glass substrates were cleaned for 1 h in a 1:1 (v/v) mixture of methanol and hydrochloric acid and activated for 30 min in concentrated sulfuric acid. After this procedure, the substrate was rinsed and washed thoroughly with Milli-Q water.

The preparation of $(PSS/NiAl)_n$ heterogeneous UTFs (**4**) was carried out following a process of layer-by-layer (LbL) deposition, consisting of a cyclic repetition of several steps: (i) dipping the activated substrate in a freshly prepared colloidal suspension (1 g L^{-1}) of LDH nanosheets in formamide for 10 min; (ii) washing the substrate in three separate baths, for 2 min in each one (the first with formamide and the other two with Milli-Q water); (iii) dipping the substrate in an aqueous solution of PSS (prepared by diluting 2 g L^{-1} of a 30 wt % water solution in Milli-Q water) for 15 min; (iv) washing the substrate in three separate Milli-Q water baths, for 2 min in each one. A multilayered UTF of $(PSS/LDH)_n$ was obtained by depositing alternatively positively charged NiAl-LDH nanosheets colloidal

dx.doi.org/10.1021/ic400734t | Inorg. Chem. 2013, 52, 6214−6222

suspensions and anionic PSS solution for n cycles. Note that each deposition cycle of both, LDH and PSS, has been defined as a unit or bilayer. Finally, the UTF was dried with a nitrogen flow at room temperature.

4. Physical Characterization. Metallic atomic composition of bulk samples was determined by means of electron probe microanalysis (EPMA) performed in a Philips Model SEM-XL30 system equipped with an EDAX microprobe. Powder X-ray diffraction (PXRD) profiles were collected at 293(2) K with a Siemens Model D-500 X-ray powder diffractometer equipped with 2.2 kW sealed Cu Kα source (λ_α = 1.54184 Å), diffracted beam monochromator, rotary sampler, and a rotating-anode Rigaku Model D-max at 80 mA and 45 kV. Samples were grounded and mounted on a flat sample plate. Typically, profiles were collected as step scans in the 5° < 2Θ < 70° range with a 0.05° step size over a period of 2.16 h. The X-ray analysis of the UTF samples were performed on a Bruker D8 Discover X-ray diffractometer with a Θ−Θ geometry equipped with a 2.2 kW Cu Kα source (λ_α = 1.54184 Å), operating at 40 kV and 40 mA. Typically, profiles were collected in the 1° < 2Θ < 15° range with a 0.05° step size and 300 s/step. A Fourier transform infrared (FT-IR) Nicolet Model 5700 spectrometer was used for transmission and ATR measurements, equipped with (i) a KBr beam splitter; (ii) two internal detectors, DTGS-KBr (4000−400 cm^{-1} spectral range) and MCT/A (4000−650 cm^{-1} spectral range); (iii) a VeeMAX II accessory (PIKE Technologies) using a flat-plate Ge 60° crystal and a manual polarizer ZnSe. Thermogravimetric analysis (TGA) of all compounds were carried out with a Mettler Toledo TGA/SDTA 851 apparatus in the temperature range of 25−800 °C under 30 mL min^{-1} of air flow and at 10 K min^{-1} scan rate. Particles morphologies and dimensions were studied via scanning electron microscopy (SEM) (Hitachi Model S-4100), using an accelerating voltage of 20 keV. The size and shape of the exfoliated LDH sheets were investigated using a Nanoscope IVa atomic force microscope (AFM) from Veeco. A dispersion of NiAl-NO_3 LDH in formamide (0.1 g L^{-1}) was deposited on silicon wafers (p-type ⟨100⟩, from DXL Enterprises, Inc.) using a spinner (Laurell Technologies Corporation, Model WS-400B-6NPP/Lite) working at 5000 rpm during 20 s. The images were obtained using tapping mode in air at room temperature with Si tips (frequency = 300 kHz and K = 40 N m^{-1}, respectively). Images were recorded with 512 × 512 pixels and a scan rate of 0.5−1 Hz. Processing and analysis of the images were carried out using the Nanotec WSXM software.[37] UV−vis absorption spectra were recorded using an Agilent Model 8453 spectrometer in the range from 190 nm to 900 nm. TEM studies were carried out using a JEOL Model JEM-2010 instrument operating at an accelerating voltage of 200 kV. A drop of the LDH colloidal suspension was placed on the TEM lacey Formvar/carbon grids and then dried at room temperature under vacuum. Dynamic light scattering (DLS) measurements were carried out with a Zetasizer Nano ZS instrument (Malvern Instruments, Ltd.) on a centrifuged solution of exfoliated LDH in formamide (1 g L^{-1}). The temperature was set at 25 ± 0.1 °C using a thermostat bath. Mean hydrodynamic diameter and correlation functions were determined by accumulative analysis. Periodical measurements over a period of 72 h, after the delamination process was finished, given the opportunity to determine the stability of the colloidal solution.

Magnetic measurements were carried out with a Quantum Design (SQUID) magnetometer (Model MPMS-XL-5), using Mylar as a diamagnetic substrate. DC magnetization studies were performed between −5 T and +5 T at a constant temperature of 2 K. The dynamic AC susceptibility data were collected from a freshly prepared $(PSS/NiAl)_n$ UTF (n = 80) in the 2−20 K range with an applied alternating field of 3.95 G at various frequencies between 1 Hz and 1000 Hz.

RESULTS AND DISCUSSION

1. Synthesis of LDHs. Based on the complementary chemical analytical data obtained through TGA (see Figure SI-1 in the Supporting Information) and EPMA, the composition of the synthesized LDH systems have been summarized in Table 1. The good agreement between the Ni/Al ratio before and after the salt-acid treatment, with the ratios used for the gel preparation indicates that no contaminant phases were formed along the synthetic procedure and no chemical composition changes occurred during the post-synthesis treatment. Yet, it is significant that the Ni/Al ratio is slightly lower than that expected from the ratio introduced in the reaction mixture, suggesting that probably some amorphous aluminum oxide could be present in the studied samples.

Table 1. Metal Ratio of the Synthetic Gels (Theoretical) and the Bulk Isolated Compounds (Experimental), as Estimated from Electronic Probe Microanalysis (EPMA)

	x^a				
	Theor	Exp	water [wt %][b]	formula weight [g]	molecular formula
(**1**) NiAl-CO_3	0.33	0.38	5.66	97.63	$[Ni_{0.62}Al_{0.38}(OH)_2](CO_3)_{0.190}\cdot 0.3H_2O$
(**2**) NiAl-NO_3	0.33	0.37	6.82	111.47	$[Ni_{0.63}Al_{0.37}(OH)_2](NO_3)_{0.370}\cdot 0.4H_2O$
(**3**) NiAl-PSS	0.33	0.35	8.89	159.94	$[Ni_{0.65}Al_{0.35}(OH)_2](PSS)_{0.350}\cdot 0.8H_2O$

[a] $x = [M^{3+}]/([M^{2+}] + [M^{3+}])$. [b] Water content deduced from the thermogravimetric analysis and corresponding calculated molecular formulae.

SEM images of the pristine NiAl-CO_3 (**1**) system and of the material that results from the salt-acid treatment NiAl-NO_3 (**2**) display uniform hexagonal platelets (Figure 1), as expected from the use of a homogeneous precipitation method, discarding drastic damages to the layers in the nitrate exchange procedure. It is worthwhile mentioning that the synthesis conditions used to reach the optimum pH guarantee a slow and homogeneous nucleation process, resulting in higher-quality materials, in terms of morphology, than those prepared by conventional coprecipitation methods. As can be seen in Figure 1, the lateral size of the hexagonal platelets is ∼0.1 μm.

Figure 2 shows the PXRD patterns of **1** prepared by the homogeneous precipitation method using HMT and their respective nitrate-intercalated derivatives **2**, obtained after salt-acid treatment. They present the expected profile for LDH systems, with no peaks related to contaminant phases, confirming the phase purity for the isolated materials. The sharp intense peaks observed at low Θ values and the less-intense ones, appearing at higher angular values, were indexed by assuming a rhombohedral structure (symmetry 3R). These data, along with the refined lattice parameters, are summarized in Table 2. The obtained basal spacing (BS) values are in excellent agreement with those expected for carbonate (7.6 Å) and nitrate (8.8 Å) intercalated LDHs.[10]

FT-IR spectrum (see Figure SI-2 in the Supporting Information) was first used to confirm the presence of carbonate ions in the interlayer space of the original LDH and, later on, to verify the quantitative substitution of carbonate with nitrate ions after the salt-acid treatment. It is worth noting that this step is of critical importance, because the exfoliation process could be limited by the presence of a contaminant carbonate phase.

2. Exfoliation of LDHs. The exfoliation of nitrate-based LDH systems has been carried out by mechanically stirring and sequential cycles of ultrasound treatment in 1 g L^{-1} formamide solutions over a period of 72 h. Next, the stability of the greenish emulsion obtained from the corresponding NiAl-NO_3

dx.doi.org/10.1021/ic400734t | Inorg. Chem. 2013, 52, 6214−6222

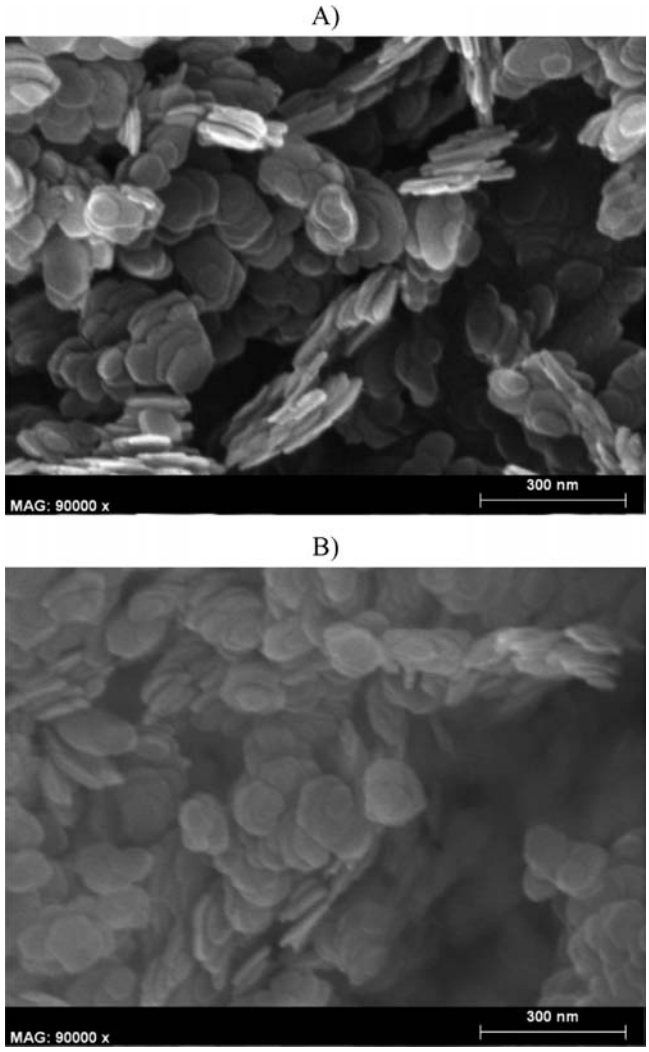

Figure 1. SEM images of (A) LDH precursor **1** and (B) LDH precursor **2**, showing the homogeneous size distribution and the hexagonal morphology of the crystals.

LDH has been studied with dynamic light scattering (DLS). Figure 3 shows the size distributions measured for the NiAl colloidal nanosheet suspensions over a period of 72 h, confirming not only that the size distribution of the exfoliated nanosheets remains constant over the studied period, but also that its size is in excellent agreement with the value estimated from the SEM study performed on the corresponding LDH-NO_3 phase (vide supra). Next, NiAl nanosheets were studied with TEM to demonstrate that no dramatic damage is introduced during the mechanical exfoliation process. Figure SI-3 in the Supporting Information shows a TEM picture of NiAl nanosheets, exhibiting equivalent hexagonal plate-like morphologies, with lateral sizes in good agreement with those estimated via SEM (for the pristine nonexfoliated materials) and DLS. Moreover, the homogeneous contrast exhibited by these lamellae is indicative of their uniform nanometric thickness.

To provide direct evidence of the presence of unilamellar layers result of the exfoliation process, atomic force microscopy (AFM) and UV−vis absorption studies were carried out. Figure 3 shows AFM images collected by spin-coating a clean silicon wafer with freshly prepared emulsions of NiAl nanosheets. The image on the left covers a 1 μm × 1 μm area and illustrates the presence of particles with platelike morphologies and lateral sizes coincident once again with the SEM/DLS experiments (vide supra). Moreover, as represented in the magnified scan on the right side of Figure 3, the profile of the NiAl-nanosheets permits estimating an average height profile of 0.76 nm, corresponding with the presence of a single unilamellar nanosheet. The observed deviation, with respect to the crystallographic thickness of a single brucite layer (0.48 nm), must be attributed to the adsorption of solvent molecules and residual counterions present in the medium, according to that generally described for previous AFM studies of exfoliated LDHs.[38] Next, UV−vis absorption spectra were collected from freshly delaminated colloidal suspensions of **2** at variable concentration. Figure 4 represents their absorbance at 374 and 642 nm as a linear function of the colloid content and their fitting to a Lambert−Beer law, indicating that these nanosheets are nearly monodispersed with almost negligible interactions[39] and supporting the presence of single monolayers, as a result of the exfoliation process.

3. Flocculated Bulk Material. Before approaching the characterization of structured multilayered architectures via LbL, we decided to study the direct combination of freshly prepared emulsions containing as-exfoliated NiAl-LDH with PSS. Besides providing initial insights on the interaction between PSS and the exfoliated LDH layers, this information enables direct comparison between both routes, therefore discarding the formation of bulk solids with poorer structural order under LbL conditions.

This preliminary test results in the rapid formation of a green solid NiAl-PSS (**3**), as a result of the flocculation of the ionic moieties in solution. The green solid **3** was filtered, dried at ambient temperature under vacuum and chemical and structurally characterized according to the same protocol described for the $(PSS/LDH)_n$ UTFs prepared by LbL.

Its XRD pattern (see Figure SI-4 in the Supporting Information) shows the typical profile for LDH systems but remarkably poorer crystallinity than the starting nonexfoliated materials, likely because of the high number of defects introduced during its rapid flocculation. Nevertheless, it is possible to distinguish both the (00*l*) peaks and the in-layer (110) peak at ∼61°. The presence of the latter indicates that the order across the brucite-like layers is retained after the exfoliation process, keeping constant the value of parameter *a* (3.02 Å). About the (00*l*) peaks, the first one (003) was the most clear and appeared at a value of $2\Theta \approx 4.2°$ (d = 2.105 nm), which was used to compare with the value obtained after the preparation of the corresponding hybrid materials in the UTF form. Changes in the chemical composition of the LDH layers were discarded on the basis of the EPMA data. The water content of **3** was estimated by analysis of its TGA (see Table 1). Finally, the presence of PSS in the solid was confirmed via its FT-IR spectrum (see Figure SI-5 in the Supporting Information), which clearly shows the presence of the characteristic vibration modes of the corresponding sulfonate groups at 1008 and 1040 cm^{-1} assigned to the symmetric stretching vibrations of the SO_3 group.

4. Magnetic Multilayered $(PSS/LDH)_n$ UTFs. The preparation of multilayered $(PSS/LDH)_n$ UTFs was performed according to the LbL technique. This procedure benefits from the presence of attractive electrostatic interactions between the corresponding charged components to enable the assembly of alternating PSS and LDH layers into highly ordered architectures. The fabrication of the UTFs started with the

dx.doi.org/10.1021/ic400734t | *Inorg. Chem.* 2013, 52, 6214−6222

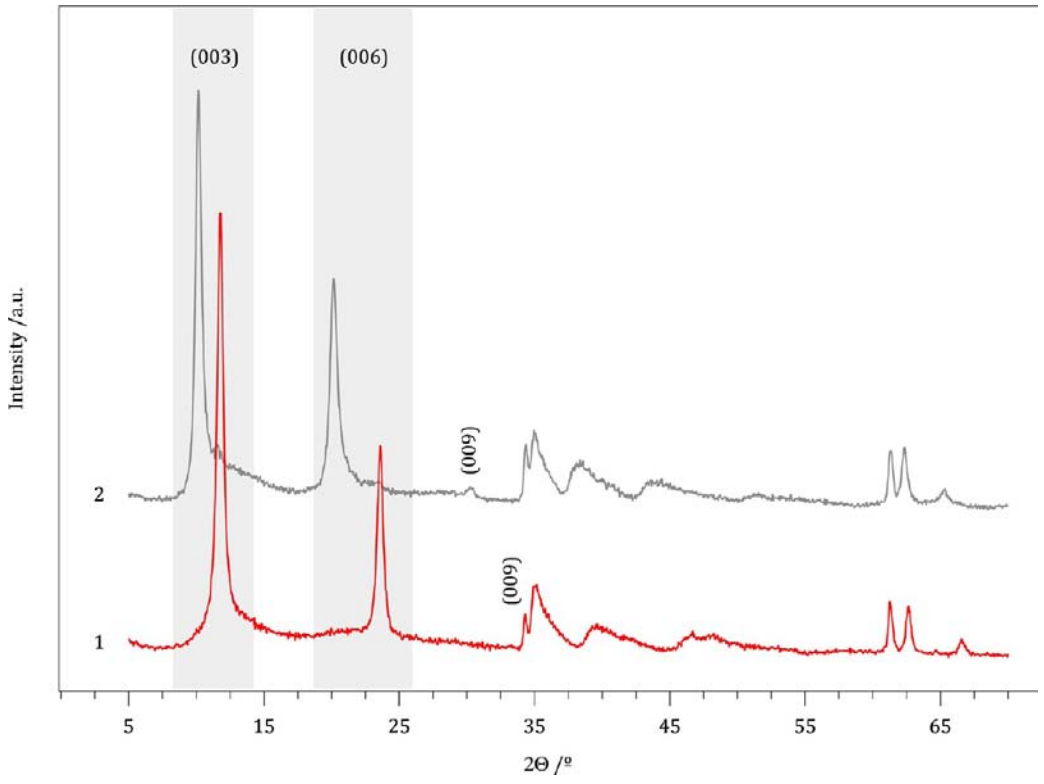

Figure 2. Powder X-ray diffraction (PXRD) pattern for LDH precursors **1** (bottom) and **2** (top).

Table 2. X-ray Diffraction Data and Unit Cell Parameters for the NiAl-LDH Precursor Systems and NiAl-PSS Ultrathin Films (UTFs)

	2Θ [deg] (*hkl*)				Calculated Parameters[a] [Å]		
LDH system	(003)	(006)	(009)	(110)	*a*	*c*	basal spacing, BS
(**1**) NiAl-CO_3	11.77	23.70	34.25	61.25	3.03	22.88	7.63
(**2**) NiAl-NO_3	10.15	20.10	29.55	61.20	3.03	26.62	8.87
(**3**) NiAl-PSS	4.27	8.98	12.63	61.39	3.02	61.41	20.47
(**4**) $(PSS/NiAl)_{80}$-UTF	4.45	9.10	13.50			59.79	19.93

[a] $a = 2d_{110}$; BS = $(d_{003} + 2d_{006} + 3d_{009})/3$.

activation of the quartz substrate in a strongly acidic medium, followed by normal alternate adsorption of NiAl-LDH nanosheets and PSS, by immersion in the corresponding LDH colloidal suspension and PSS solution, respectively. After defining the optimal conditions for deposition, such as the time of every immersion, the order of these immersions, the number of washing solutions, etc., the growth of $(PSS/LDH)_n$ multilayer UTFs was monitored by UV−vis absorption spectra.

Because of a big mismatch of the absorption coefficients of PSS solutions (see Figure SI-6 in the Supporting Information), in comparison with those of the LDH suspensions (see Figure 4), the UV−vis profile of $(PSS/NiAl)_n$ (**4**) is greatly dominated by the absorption features characteristic of the organic polymer. Thus, the absorption bands centered at 262 nm (see Figure SI-7 in the Supporting Information) were chosen for assessing the LbL progress. As a matter of fact, the 262 nm shoulder was the only distinguishable feature that did not saturate the photodiode response up to 80 bilayers. Figure SI-7 in the Supporting Information shows a good fitting to a linear regime of the absorbance of **4** at 262 nm with the increasing number of bilayers, up to a maximum of 80 bilayers ($R = 0.99$).

Moreover, FT-IR ATR measurements have been used for monitoring the LbL process. Figure 5 illustrates the increment of the intensity of the symmetric stretching vibration mode of the SO_3 group (centered at 1040 cm^{-1}) belonging to the PSS unit upon consecutive deposition. The fitting to a linear regime ($R = 0.98$) confirms the reproducibility and homogeneity of the deposition procedure.

The good results obtained by IR and UV−vis support the reproducibility of the deposition process in each bilayer or, in other words, a stepwise and regular deposition procedure with almost equal amounts of PSS and LDH nanosheets incorporated in each bilayer. In this context, we would like to highlight that, although the growth control on most of the previous studies on the design of layered UTFs via LbL has been limited to UV−vis studies on a remarkably smaller number of deposition cycles, until ∼30 or 50 bilayers at best,[13d,35] we have been able to confirm the reproducibility of this methodology for multilayered UTFs containing 80 bilayers through a couple of complementary techniques. The use of a polymer material instead a discrete molecule, which provides the possibility to prepare more homogeneous layers and especially the size and the good quality of the NiAl-LDH layers, could be responsible for the success in the preparation of this multilayered material with a high number of layers.

dx.doi.org/10.1021/ic400734t | *Inorg. Chem.* 2013, 52, 6214−6222

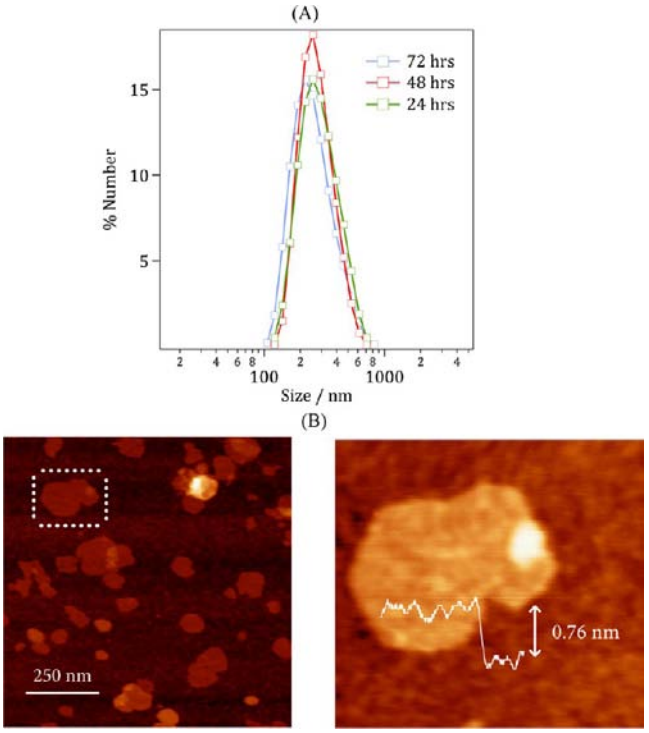

Figure 3. (A) Dynamic light scattering (DLS) size distribution of the delaminated NiAl-LDH (**2**) in formamide (1 g L^{-1}), over a period of 72 h, after finishing the delamination process. (B) Tapping-mode atomic force microscopy (AFM) image of the exfoliated NiAl-LDH nanosheets deposited by spin coating on a silicon wafer substrate. (C) Height profile of a NiAl-LDH nanosheet concordant with the expected value.

From a structural point of view, $(PSS/NiAl)_n$ UTFs exhibit analogous XRD patterns with the typical LHD-like profile but broader Bragg peaks when compared to the pristine LDH starting precursors. Three diffraction peaks (see Figure 6), which can be indexed as (003), (006), and (009) reflections by assuming a rhombohedral unit cell (see Table 2), are observed at low 2Θ values for $(PSS/NiAl)_{80}$, thus supporting a multilayered architecture with periodic repetition of bilayers of inorganic LDH layers and the polymer. Given that these peaks are related to the stacking periodicity of the arranged layers along the *c*-axis, they permit one to estimate a basal spacing of 1.993 nm. This gallery height is not only in excellent agreement with the value of 2.1 nm reported by Oriakhi et al. for a nanocomposite of LDH-PSS synthesized via in situ coprecipitation,[40] but also comparable with that estimated for the sample obtained by flocculation (2.047 nm, vide supra). The small deviation between this former value and that corresponding to the LbL-assembled UTF is likely due to the fast precipitation of the solid during the flocculation process, which typically produces less-crystalline solids with a higher amount of solvent molecules within the interlayer space.

In addition, we have been able to monitor the increase of the intensity of these (00*l*) peaks with the increasing number of bilayers (see Figure 6, left), supporting once again the progressive growth of these multilayered architectures. Although for a small number of bilayers ($n \leq 10$), the diffraction peaks observed are broad and poorly defined, the intensity of the peaks increases with the growing number of bilayers, thus supporting the formation of an ordered hybrid superstructure via regular arrangement of the layers. This suggests that the deposition process worked correctly, despite the fact that many defects could be present in the UTF.

To confirm that the intrinsic magnetic properties of the bulk NiAl-LDH material can be effectively transferred to the multilayered assembly, we studied the dynamic magnetic response of a freshly prepared $(PSS/NiAl)_n$ UTF via the deposition of 80 bilayers onto a diamagnetic Mylar substrate. Figure 7 shows the alternating current (AC) measurements as collected between 2 K and 20 K with an applied field of 3.95 G oscillating between 10 Hz and 1000 Hz. The in-phase signal (χ') clearly exhibits an exponential increase that is accompanied

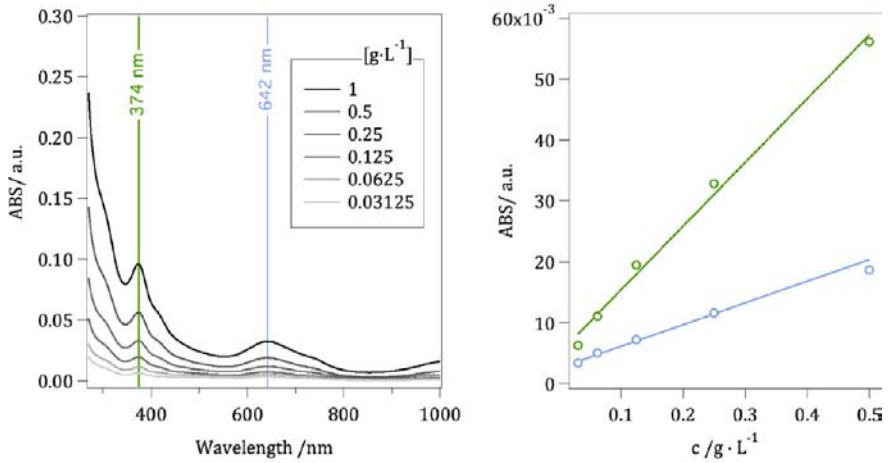

λ /nm	374	642
ε /cm^{-1}·g^{-1}·L	0.105 ± 0.005	0.036 ± 0.002

Figure 4. UV−visible absorption spectra of the colloidal suspensions of NiAl-LDH at different concentrations: 1.00, 0.50, 0.25, 0.125, 0.0625, and 0.03125 g L^{-1}. The right side of the figure shows the fitting of the absorbance at 374 and 642 nm as a function of the nanosheets content. Bottom table shows the coefficients of NiAl-LDH suspensions.

dx.doi.org/10.1021/ic400734t | *Inorg. Chem.* 2013, 52, 6214−6222

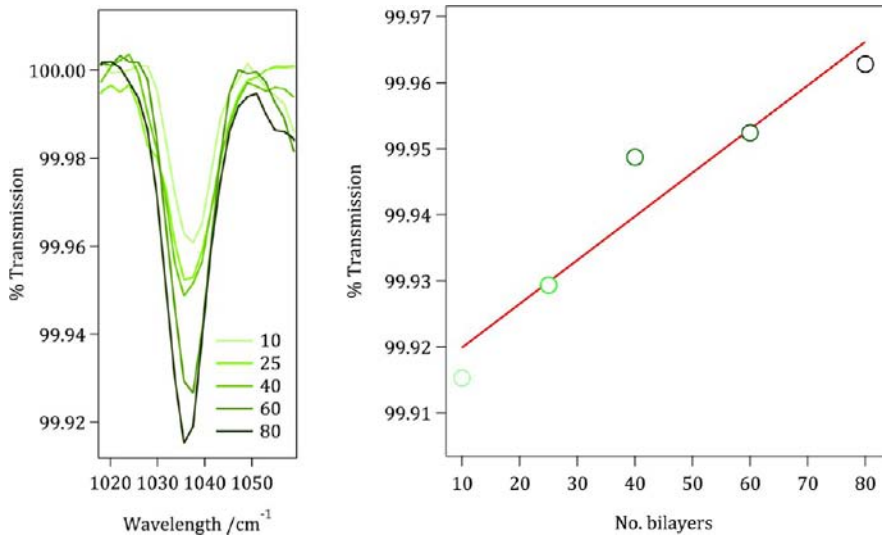

Figure 5. Evolution of the peak associated with the sulfonate group of the PSS in the IR spectra of NiAl-PSS$_n$ ultrathin films (n = 10−80). The right side of the figure shows the correlation between the percentage transmission corresponding to the sulfonate group and the number of bilayers.

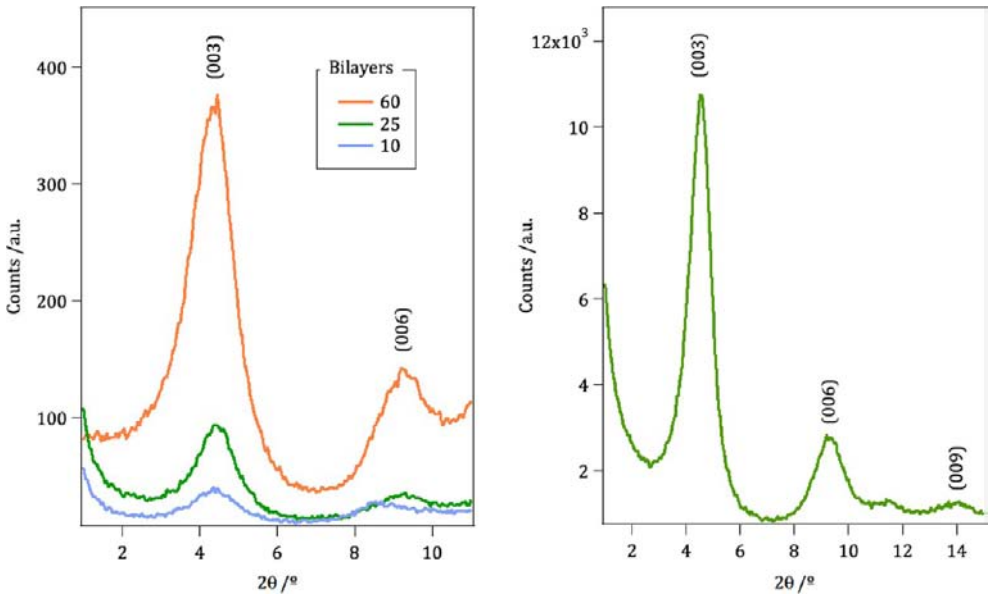

Figure 6. (Right) X-ray diffraction (XRD) pattern for an 80-bilayer system (the NiAl-PSS$_{(80)}$ ultrathin film (UTF)). (Left) Evolution of XRD patterns for the NiAl-PSS$_n$ UTFs at 10, 25, and 60 bilayers.

by a positive response of the out-of-phase signal (χ'') below 5 K, as expected for the onset of long-range magnetic correlation across the LDH layers. The DC magnetization rapidly increases with the applied field at 2 K up to 5 T where it reaches saturation and defines a plateau, thus confirming the ferromagnetic nature of the magnetic exchange between the octahedral Ni(II) ions, as mediated by the hydroxyl bridges in the LDH layers (see Figure SI-8 in the Supporting Information). The coercive field extracted from hysteresis loop collected at 2 K is below 0.1 kG, which is in good agreement with the soft magnetic nature of the bulk NiAl-LDH (see Figure SI-8 in the Supporting Information). The temperature for which spontaneous magnetization is observed in the UTF is also consistent with the magnetic behavior of the bulk LDH, because this material behaves as a ferromagnet from 5.2 K in the solid state, when the LDH sheets are interleaved with nitrate anions.[15] While the position of the χ' and χ'' peaks does not depend on the frequency of the oscillating of the magnetic field for the bulk solid, this is not the case for the UTF, which exhibits clear dependence for both signals. This temperature shift can be quantified by using the parameter φ, which can be calculated[41] using the expression

$$\varphi = \frac{\Delta T_f}{\Delta(T_f \log \omega_i)}$$

with T_f being the temperature corresponding to the maximum in the χ'' signal for a given frequency value (ω_i), and ΔT_f represents the interval of temperatures covered by the T_f values for the minimum and maximum frequencies. Given that, for spin glasses, φ typically oscillates between 0.001 and 0.1, the obtained value of 0.08 is indicative of glassy behavior. Despite the crystallinity of the assembled superstructure in the UTF, the origin of this glassiness is likely associated with the structural disorder introduced upon the LbL process that might

dx.doi.org/10.1021/ic400734t | Inorg. Chem. 2013, 52, 6214−6222

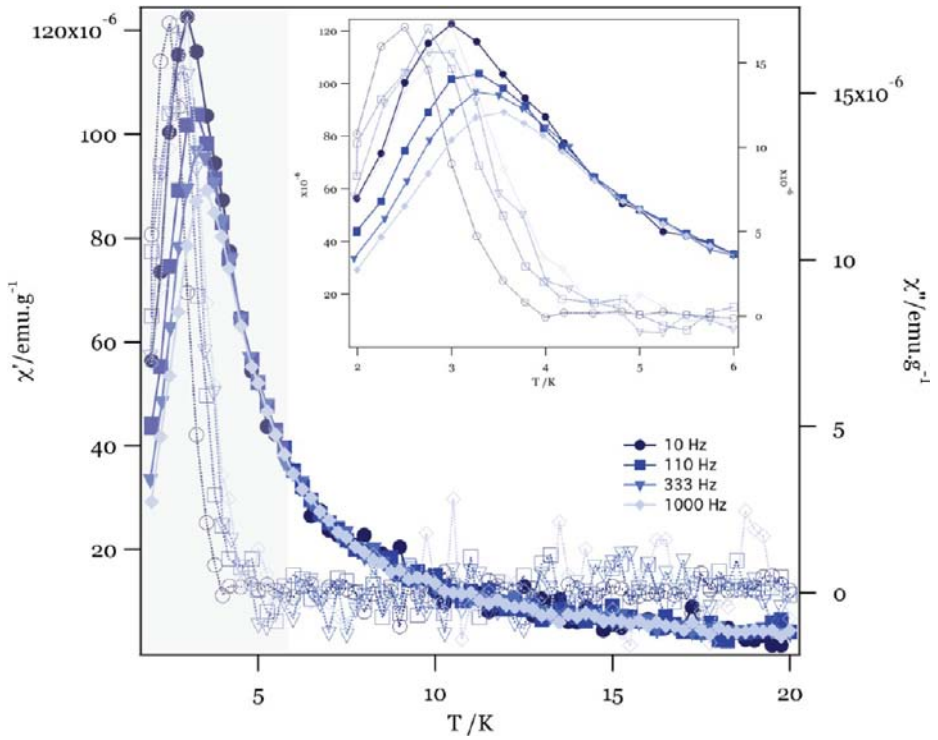

Figure 7. AC magnetic measurements for the NiAl-PSS_{80} UTF collected between 2 K and 20 K with an applied field of 3.95 G oscillating between 10 and 1000 Hz. The inset shows an expanded view of the temperature interval for which the onset of spontaneous magnetization is observed. In-phase susceptibility and out-of-phase signals are represented by filled and empty symbols, respectively. Solid lines are present only to serve as a guide for the eye.

be affecting the relative orientation the layers. Other potential factors, such as changes affecting the chemical composition or the internal order of the magnetic layers must be discarded in the light of the chemical/structural analysis of the exfoliated layers, which confirms the belief that their nature remains identical to that of the LDH layers in the bulk (vide supra).

CONCLUSIONS

In a first stage, we have synthesized homogeneous hexagonal platelets of NiAl-CO_3 layered double hydroxide (LDH) using a modified homogeneous precipitation method. The as-made material was successfully exchanged with nitrate anions and then exfoliated in formamide to produce steady dispersions of cationic two-dimensional (2D) sheets with nanometric thickness (ca. 0.75 Å). Next, these have been used as macromolecular building blocks, along with PSS, to build hybrid $(PSS/NiAl)_n$ ultrathin films (UTFs) via a layer-by-layer (LbL) process. The UTF growing process has been monitored with UV−vis, FT-IR, and XRD to confirm the sequential deposition of bilayers and the appearance of long-range stacking order in the multilayered architecture. The magnetic properties of the UTF have been studied using Mylar as a diamagnetic substrate and compared with the magnetic behavior of the pristine LDH. Our data reveal that the magnetic features of the assembled superstructure remain close to those of the parent LDH with the onset of spontaneous magnetization at low temperatures (ca. 5 K), as a result of the ferromagnetic exchange between Ni(II) centers across the LDH layers. In turn, the AC measurements show some differences as the χ' and χ'' signals exhibit a clear frequency dependence that can be associated to glassy-like behavior, according to the calculated Mydosh parameters. This likely originates from the additional degree of disorder introduced in the UTF assembly upon LbL deposition. This magnetic behavior is consistent with the low-temperature magnetism intrinsic to LDH hosts, in contrast with the anomalous room-temperature magnetic response recently reported for NiFe-LDH magnetic films that can be rather ascribed to the presence of contaminant iron oxide.[42]

This work demonstrates that physical properties intrinsic to bulk macroscopic solids, such as the magnetism of LDH hosts incorporating paramagnetic transition-metal ions, can be effectively transferred to nanostructured architectures by LbL sequential deposition of the 2D cationic nanosheets that result from their exfoliation. To the best of our knowledge, this is the first example describing the LbL assembly of magnetic LDH-based nanostructures and represents a significant advance toward the miniaturization of magnetic devices based on thin films. We are currently exploring the preparation of more-complex multifunctional UTFs that combine the magnetism of LDHs with the superconductivity provided by single layers of cationic layered chalcogenides.

ASSOCIATED CONTENT

Supporting Information

This material is available free of charge via the Internet at http://pubs.acs.org.

AUTHOR INFORMATION

Corresponding Author

*Tel.: +44 (0) 151 794 3583. Fax: +44 (0) 151 794 3528. E-mail: gastaldo@liverpool.ac.uk.

Notes

The authors declare no competing financial interest.

dx.doi.org/10.1021/ic400734t | Inorg. Chem. 2013, 52, 6214−6222

■ ACKNOWLEDGMENTS

Financial support from the European Union (EU) (Projects HINTS and ERC Advanced Grant SPINMOL), the Spanish MINECO (Project Consolider-Ingenio in Molecular Nanoscience CSD2007-00010 and Project Nos. MAT2007-61584, MAT2011-22785 and CTQ-2011-26507), and the Generalitat Valenciana (Prometeo and ISIC-NANO Programs) are gratefully acknowledged. C.M.-G. thanks the EU for a Marie Curie Fellowship (No. IEF-253369). We also acknowledge J. V. Usagre, J. M. Martínez, and G. Agustí for assistance with the synthesis and magnetic measurements.

■ REFERENCES

(1) Cornia, A.; Mannini, M.; Sainctavit, P.; Sessoli, R. *Chem. Soc. Rev.* **2011**, *40*, 3076.
(2) Mannini, M.; Pineider, F.; Danieli, C.; Totti, F.; Sorace, L.; Sainctavit, Ph; Arrio, M. A.; Otero, E.; Joly, L.; Cezar, J. C.; Cornia, A.; Sessoli, R. *Nature* **2010**, *468*, 417.
(3) Martínez, R. V.; García, F.; García, R.; Coronado, E.; Forment-Aliaga, A.; Romero, F. M.; Tatay, S. *Adv. Mater.* **2007**, *19*, 291.
(4) Cavallini, M.; Gómez-Segura, J.; Ruiz-Molina, D.; Massi, M.; Albonetti, C.; Rovira, C.; Veciana, J.; Biscarini, F. *Angew. Chem., Int. Ed.* **2005**, *44*, 888.
(5) Martínez, R. V.; Martínez, J.; Chiesa, M.; Garcia, R.; Coronado, E.; Pinilla-Cienfuegos, E.; Tatay, S. *Adv. Mater.* **2010**, *22*, 588.
(6) Coronado, E.; Martí-Gastaldo, C.; Galan-Mascaros, J. R.; Cavallini, M. *J. Am. Chem. Soc.* **2010**, *132*, 5456.
(7) Talham, D. R. *Chem. Rev.* **2004**, *104*, 5479.
(8) Fried, T.; Shemer, G.; Markovich, G. *Adv. Mater.* **2001**, *13*, 1158.
(9) (a) Clemente-León, M.; Mingotaud, C.; Agricole, B.; Gómez-Garcia, C. J.; Coronado, E.; Delhaès, P. *Angew. Chem., Int. Ed.* **1997**, *36*, 1114. (b) Coronado, E.; Mingotaud, C. *Adv. Mater.* **1999**, *11*, 869. (c) Clemente-León, M.; Coronado, E.; Delhaes, P.; Gómez-García, C. J.; Mingotaud, C. *Adv. Mater.* **2001**, *13*, 574. (d) Clemente-León, M.; Coronado, E.; Gómez-García, C. J.; Mingotaud, C.; Ravaine, S.; Romualdo-Torres, G.; Delhaès, P. *Chem.—Eur. J.* **2005**, *11*, 3979. (e) Clemente-León, M.; Coronado, E.; Soriano-Portillo, A.; Mingotaud, C.; Dominguez-Vera, J. M. *Adv. Colloid Interface Sci.* **2005**, *116*, 193.
(10) Cavani, F.; Trifiro, F.; Vaccari, A. *Catal. Today* **1991**, *11*, 173.
(11) Clearfield, A. *Chem. Rev.* **1988**, *88*, 125.
(12) Wang, J.; Kalinichev, A. G.; Kirkpatrick, R. J.; Hou, X. *Chem. Mater.* **2001**, *13*, 145.
(13) (a) Costantino, U.; Marmottini, F.; Nocchetti, M.; Vivani, R. *Eur. J. Inorg. Chem.* **1998**, 1439. (b) Ogawa, M.; Kaiho, H. *Langmuir* **2002**, *18*, 4240. (c) Adachi-Pagano, M.; Forano, C.; Besse, J.-P. *J. Mater. Chem.* **2003**, *13*, 1988. (d) Liu, Z. P.; Ma, R. Z.; Osada, M.; Iyi, N.; Ebina, Y.; Takada, K.; Sasaki, T. *J. Am. Chem. Soc.* **2006**, *128*, 4872. (e) Liu, Z.; Ma, R.; Ebina, Y.; Iyi, N.; Takada, K.; Sasaki, T. *Langmuir* **2007**, *23*, 861. (f) Naghash, A.; Etsell, T. H.; Lu, B. *J. Mater. Chem.* **2008**, *18*, 2562.
(14) (a) Adachi-Pagano, M.; Forano, C.; Besse, J.-P. *Chem. Commun.* **2000**, *91*. (b) O'Leary, S.; O'Hare, D.; Seeley, G. *Chem. Commun.* **2002**, 1506. (c) Li, L.; Ma, R.; Ebina, Y.; Iyi, N.; Sasaki, T. *Chem. Mater.* **2005**, *17*, 4386. (d) Wu, Q. L.; Olafsen, A.; Vistad, O. B.; Roots, J.; Norby, P. *J. Mater. Chem.* **2005**, *15*, 4695. (e) Ma, R. Z.; Liu, Z. P.; Li, L.; Iyi, N.; Sasaki, T. *J. Mater. Chem.* **2006**, *16*, 3809. (f) Abellán, G.; Coronado, E.; Martí-Gastaldo, C.; Pinilla-Cienfuegos, E.; Ribera, A. *J. Mater. Chem.* **2010**, *20*, 7451.
(15) Coronado, E.; Marti-Gastaldo, C.; Navarro-Moratalla, E.; Ribera, A.; Blundell, S. J.; Baker, P. J. *Nat. Chem.* **2010**, *2*, 1031.
(16) Zhao, J.-W.; Kong, X.-G.; Shi, W.-Y.; Shao, M.-F.; Han, J.-B.; Wei, M.; Evans, D. G.; Duan, X. *J. Mater. Chem.* **2011**, *21*, 13926.
(17) Shi, W.; Ji, X.; Zhang, S.; Wei, M.; Evans, D. G.; Duan, X. *J. Phys. Chem. C* **2011**, *115*, 20433.
(18) Ma, R.; Sasaki, T. *Adv. Mater.* **2011**, *22*, 5082.
(19) Decher, G.; Hong, J. D. *Makromol. Chem., Macromol. Symp.* **1991**, *46*, 321.
(20) Iler, R. K. *Colloid. J.* **1966**, *21*, 569.
(21) Zhang, X.; Chen, H.; Zhang, H. *Chem. Commun.* **2007**, 1395.
(22) Podsiadlo, P.; Michel, M.; Lee, J.; Verploegen, E.; Kam, N. W. S.; Ball, V.; Lee, J.; Qi, Y.; Hart, A. J.; Hammond, P. T.; Kotov, N. A. *Nano Lett.* **2008**, *8*, 1762.
(23) Manga, K. K.; Zhou, Y.; Yan, Y.; Loh, K. P. *Adv. Funct. Mater.* **2009**, *19*, 3638.
(24) Shen, J.; Hu, Y.; Li, C.; Qin, C.; Shi, M.; Ye, M. *Langmuir* **2009**, *25*, 6122.
(25) (a) Sasaki, T.; Ebina, Y.; Tanaka, T.; Harada, M.; Watanabe, M.; Decher, G. *Chem. Mater.* **2001**, *13*, 4661. (b) Zhou, Y.; Ma, R.; Ebina, Y.; Takada, K.; Sasaki, T. *Chem. Mater.* **2006**, *18*, 1235. (c) Li, L.; Ma, R.; Ebina, Y.; Fukuda, K.; Takada, K.; Sasaki, T. *J. Am. Chem. Soc.* **2007**, *129*, 8000. (d) Dong, X.; Osada, M.; Ueda, H.; Ebina, Y.; Kotani, Y.; Ono, K.; Ueda, S.; Kobayashi, K.; Takada, K.; Sasaki, T. *Chem. Mater.* **2009**, *21*, 4366.
(26) Han, J. B.; Lu, J.; Wei, M.; Wang, Z. L.; Duan, X. *Chem. Commun.* **2008**, 5188.
(27) Hornok, V.; Erdohelyi, A.; Dekany, I. *Colloid Polym. Sci.* **2005**, *283*, 1050.
(28) Huang, S.; Cen, X.; Peng, H.; Guo, S.; Wang, W.; Liu, T. *J. Phys. Chem. B* **2009**, *113*, 15225.
(29) Szekeres, M.; Szechenyi, A.; Stepan, K.; Haraszti, T.; Dekany, I. *Colloid Polym. Sci.* **2005**, *283*, 937.
(30) Yan, D.; Lu, J.; Wei, M.; Han, J.; Ma, J.; Li, F.; Evans, D. G.; Duan, X. *Angew. Chem., Int. Ed.* **2009**, *48*, 3073.
(31) Guo, X.; Zhang, F.; Evans, D. G.; Duan, X. *Chem. Commun.* **2010**, *46*, 5197.
(32) Han, J.; Dou, Y.; Wei, M.; Evans, D. G.; Duan, X. *Angew. Chem., Int. Ed.* **2010**, *49*, 2171.
(33) Bendall, J. S.; Paderi, M.; Ghigliotti, F.; Li Pira, N.; Lambertini, V.; Lesnyak, V.; Gaponik, N.; Visimberga, G.; Eychmueller, A.; Torres, C. M. S.; Welland, M. E.; Gieck, C.; Marchese, L. *Adv. Funct. Mater.* **2010**, *20*, 3298.
(34) Li, S.; Lu, J.; Ma, H.; Xu, J.; Yan, D.; Wei, M.; Evans, D. G.; Duan, X. *Langmuir* **2011**, *27*, 11501.
(35) Yan, D.; Lu, J.; Wei, M.; Evans, D. G.; Duan, X. *J. Mater. Chem.* **2011**, *21*, 13128.
(36) Iyi, N.; Matsumoto, T.; Kaneko, Y.; Kitamura, K. *Chem. Mater.* **2004**, *16*, 2926.
(37) Horcas, I.; Fernéndez, R.; Gómez-Rodríguez, J. M.; Colchero, J.; Gómez-Herrero, J.; Baro, A. M. *Rev. Sci. Instrum.* **2007**, *78* (1), 013705.
(38) Pedersen, H.; Ojamaee, L. *Nano Lett.* **2006**, *6*, 2004.
(39) Sasaki, T.; Watanabe, M. *J. Phys. Chem. B* **1997**, *101*, 10159.
(40) Oriakhi, C. O.; Farr, I. V.; Lerner, M. M. *J. Mater. Chem.* **1996**, *6*, 103.
(41) Mydosh, J. A. *Spin Glasses: An Experimental Introduction*; Taylor & Francis: London, 1993.
(42) (a) Dou, Y.; Liu, X.; Shao, M.; Han, J.; Wei, M. *J. Mater. Chem. A* **2013**, *1*, 4786−4792 (DOI: 10.1039/c3ta01674a). (b) Abellán, G.; Carrasco, J. A.; Coronado, E. submitted.